Liquid-Phase Electrochemical Scanning Electron Microscopy for In Situ Investigation of Lithium Dendrite Growth and Dissolution

*Genlan Rong, Xinyi Zhang, Wen Zhao, Yongcai Qiu, Meinan Liu, Fangmin Ye, Yan Xu, Jiafan Chen, Yuan Hou, Wanfei Li, Wenhui Duan, and Yuegang Zhang**

Lithium batteries represent the most promising energy storage technology and have been studied extensively.[1–9] However, lithium dendrite growth is one of the most critical obstacles that hinder the development of high capacity lithium metal anodes.[9,10] In this work, we developed an in situ electrochemical scanning electronic microscopy (EC-SEM) method to systematically study the lithium plating/stripping processes in liquid electrolytes. The results demonstrate that the lithium dendrite growth speed and mechanism is greatly affected by the additives in the electrolytes. A co-addition of both lithium nitrate and lithium polysulfide in the ether-based electrolyte minimizes the dendrite growth and results in a smooth lithium surface. The direct EC-SEM observation of "dead" lithium formation even during the lithium deposition process provides strong evidence that lithium dendrites are etched by lithium polysulfides in the electrolyte. As revealed by the density functional theory (DFT) calculation, the dendrite etching mechanism is attributed to the lower energy of a lithium atom in lithium polysulfide clusters than that in lithium metal.

Recently, in situ microscopic tools, including transmission electron microscopy (TEM), scanning electron microscopy (SEM), and optical microscopy, are used to investigate the electrochemical processes in specifically modified cells.[11–14] For the in situ TEM investigation at a high spacial resolution,[15–18] however, the cell has to be reduced to a dimension so small that it differs too much from a real battery. For example, a nanobattery based on a liquid cell is composed of a small amount of active materials (e.g., only a few nanowires) and electrolyte, and thus could be operated for no more than ten cycles.[19] Some researchers performed in situ TEM studies on lithium metal-based batteries using an ionic liquid electrolyte or even a solid-state electrolyte, where the real interactions between the liquid electrolyte and active materials are completely missing. In addition, the highly energetic electron beam in a TEM can cause significant artifacts, such as melting of the lithium metal into liquid.[20] In contrast, in situ optical microscopy characterization[14,21–25] can provide more real information of lithium dendrite growth process due to the much larger dimension of the cells and is free from the electron beam effect. However, the resolution of an optical microscope is normally too low to provide the detailed information on the initial stage of lithium dendrites nucleation as well as during the lithium plating/stripping processes. In this respect, SEM seems to be a good compromise between the cell size (similar to that used in an optical microscope) and the resolution (down to a few nanometers). However, so far, SEM characterizations for lithium batteries were mostly carried out as ex situ,[26–32] no in situ work has been reported except that from our group.[13]

The schematic design of the EC-SEM liquid cell in this work is shown in **Figure 1**a. It is composed of two chips: a top silicon chip with a SiN_x membrane viewing window and a bottom chip made of quartz with two injection orifices. A pair of Cu current collectors and Li electrodes was patterned on the top chip with a microgap lying in the middle of the viewing window. The two chips were sealed by epoxy, with a separation of ≈0.5 mm. The orifices were also sealed with the same epoxy after the injection of the liquid electrolyte (≈60 µL). A detailed description on the fabrication of the EC-SEM liquid cell can be found in the Supporting Information. During in situ electrochemical experiments, the growth and dissolution of lithium dendrites at the edges of the Li/Cu electrodes can be observed through the SiN_x window by SEM (Figure 1b).

Using the EC-SEM liquid cell, we systematically studied the effects of lithium nitrate ($LiNO_3$) and/or lithium polysulfide (Li_2S_8) additives on the lithium dendrite growth in an electrolyte (1.0 M lithium bis(trifluoromethane sulfonyl) imide (LiTFSI) in 1,3-dioxolane (DOL) and 1,2-dimethoxyethane (DME) (volume ratio 1:1)) typically used for lithium/sulfur (Li/S) batteries. A current density of ±0.15 mA cm^{-2} was employed in all lithium plating/stripping experiments. Figure S1 (Supporting Information) shows an SEM image of the Li/Cu electrode of a bright contrast inside the EC-SEM liquid cell, which typically contains a darker edge indicative of a small gap between the Li/Cu electrode and the SiN_x membrane. The electrolyte was observed to change from a dark contrast to dark gray within only a few frames of electron

G. Rong, Dr. X. Zhang, Dr. Y. Qiu, Dr. M. Liu, Dr. F. Ye, Y. Xu, J. Chen, Y. Hou, Dr. W. Li, Prof. Y. Zhang
i-Lab
Suzhou Institute of Nano-Tech and Nano-Bionics
Chinese Academy of Sciences
Suzhou, Jiangsu 215123, China
E-mail: ygzhang2012@sinano.ac.cn,
yuegang.zhang@tsinghua.edu.cn
Dr. W. Zhao, Dr. Y. Qiu, Prof. W. Duan, Prof. Y. Zhang
Department of Physics
Tsinghua University
Beijing 100084, China

DOI: 10.1002/adma.201606187

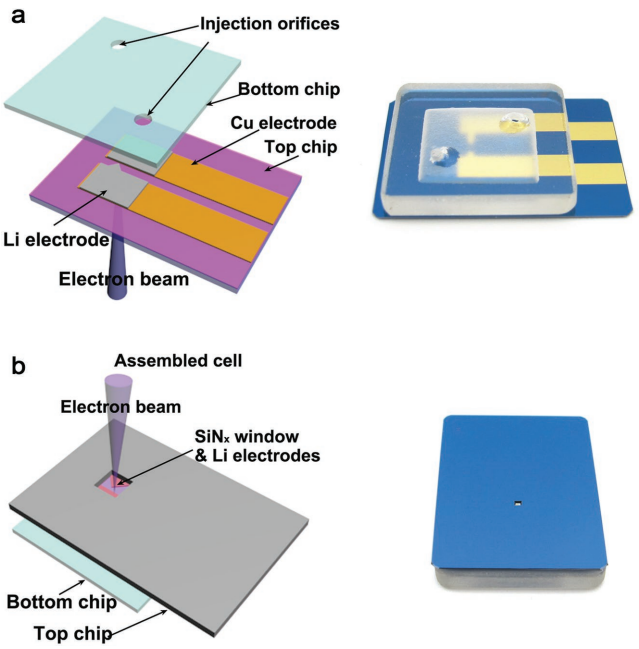

Figure 1. Schemes and photos of an in situ SEM-EC liquid cell: a) bottom and b) top views.

beam scanning, because of the charging effect of the SiN_x membrane and electrolyte. Figure S2 (Supporting Information) shows a time lapse series of SEM images revealing the lithium plating process using the LiTFSI/DOL/DME electrolyte with no additive. The contrast of the deposited lithium is dark, which is reasonable due to its low atomic number as well as the charging effect of the SiN_x membrane.[33] Dark spots near the edge of the Li/Cu electrode (blue arrow in Figure S2a, Supporting Information) were also lithium deposited in the gap between the electrode and the SiN_x membrane. The lithium dendrites became observable after plating of a few seconds, and then grew rapidly and became mossy, reaching a length of ≈60 µm after 300 s of plating (Figure S2c, Supporting Information). This indicates that lithium dendrites can form and grow easily in the LiTFSI/DOL/DME electrolyte during the plating process (video of the plating process, see Movie S1, Supporting Information).

Figure 2 shows the first cycle of lithium plating/stripping processes using the LiTFSI/DOL/DME electrolyte with the additive of $LiNO_3$ (1 wt%). The images are mapped with false color, in order to enhance the contrast of Li dendrites. The corresponding original images and video of the plating/stripping processes can be found in Figure S3 and Movie S2 (Supporting Information), respectively. The lithium dendrites were observed to grow to a length of ≈18 µm after 350 s of plating (Figure 2a–c and Figure S3a–c, Supporting Information), and then dissolved under a reversed current along with the appearance of charge accumulation (shown as the growing bright contrast) in the electrolyte (Figure 2d–f and Figure S3d–f, Supporting Information). It was observed that still some of the lithium dendrites remained even after 600 s of stripping (Figure 2f), and some even stayed unchanged between Figure 2e,f, as indicated by the white arrows in Figure 2d–f. It is very likely that those remnant lithium were electrically insulated from the electrode due to the lithium dendrite dissolution. We used the name of "dead" lithium because it is

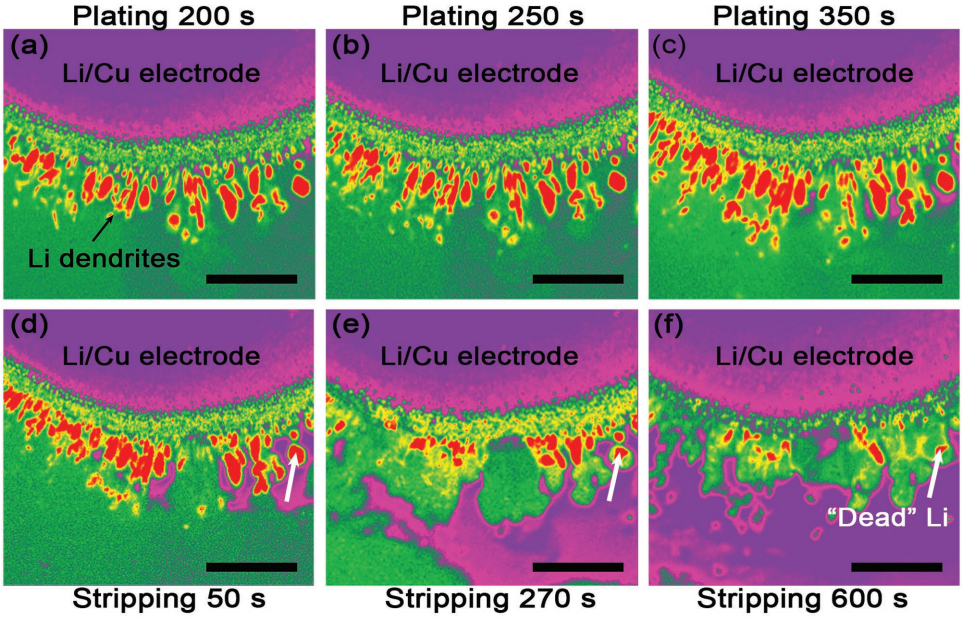

Figure 2. A time lapse series of SEM images of the processes of a–c) lithium plating and d–f) stripping under 0.15 mA cm^{-2} on the Li/Cu electrode using the LiTFSI/DOL/DME electrolyte with the additive of $LiNO_3$ (1 wt%). The artificial colors of purple-green-yellow-red represent the different contrasts from bright to dark in grayscale. The bright contrasts of Li/Cu electrode and the charged area are colored in purple, and the dark contrasts of lithium dendrites are colored in red and yellow. Scale bar: 20 µm.

electrochemically inactive during further cycling. The dendrite growth and dissolution processes are schematically illustrated in Figure S4 (Supporting Information).

With the addition of $LiNO_3$ in the LiTFSI/DOL/DME electrolyte, the formed lithium dendrites were less dense and much shorter than that in the electrolyte without any additive (Figure S2c, Supporting Information). A comparison of the lithium dendrites growth speed in different electrolytes is shown in Figure S5 (Supporting Information). It should also be noted that the dendrite growth in the $LiNO_3$ added electrolyte is not homogeneous, as shown in Figures S6 and S7 (Supporting Information). Figure S7a–d (Supporting Information) shows the nondendrite growth of a lithium layer over a region of a few tens of micrometers, while some Li dendrites also appear at the right side of the images after 80 s of plating. After 190 s of plating, more Li dendrites were found in the nearby region of the previously scanned area (see the montage of two SEM images in Figure S7e, Supporting Information). The suppression of dendrite formation in some region infers that the addition of $LiNO_3$ in electrolytes may facilitate the formation of an SEI film[32,34] on the surface of Li electrode. However, the phenomenon of inhomogeneous dendrite growth indicates that such SEI film is not uniform or not stable. As a result, $LiNO_3$ alone is not effective enough to protect the lithium anode surface for long-term cycling in a lithium battery.

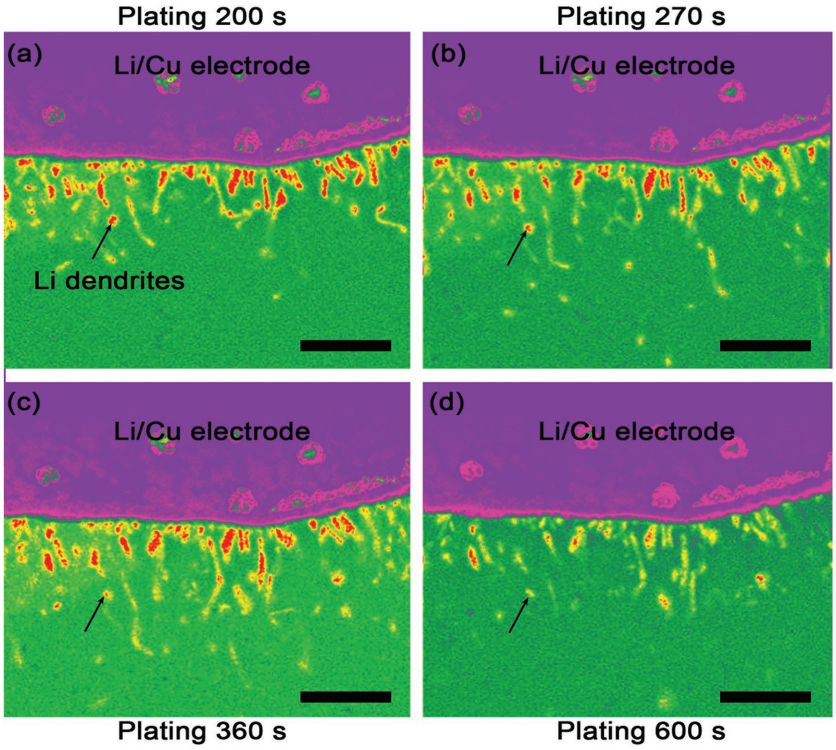

Figure 3. a–d) A time lapse series of SEM images of the lithium plating process under 0.15 mA cm^{-2} on the Li/Cu electrode using the LiTFSI/DOL/DME electrolyte with the addition of Li_2S_8 (0.2 M). The artificial colors of purple-green-yellow-red represent the different contrasts from bright to dark in grayscale. The dark contrasts of lithium dendrites are colored in red and yellow, showing their growth and etching process. Scale bar: 10 µm.

The role of Li_2S_8 additive (0.2 M) on lithium dendrite growth was also investigated (false colored **Figure 3**, see also Figure S8, Supporting Information, for original images and Movie S3, Supporting Information). At the first plating process, it can be observed that the length of the formed lithium dendrite reaches to ≈10 µm after 600 s of plating. Compared with the dendrites formed in the LiTFSI/DOL/DME electrolyte, the dendrite density in this system is much lower and their lengths are much shorter. Further investigation on this process revealed that the lengths of a few branches were beyond ≈15 µm after 270 s of plating (Figure 3b). However, it is rather abnormal that during the plating from 360 (Figure 3c) to 600 s (Figure 3d), the amount of lithium dendrites reduced significantly. The dissolution of the lithium dendrites caused some of the lithium dendrite segments disconnected to the electrode and remained unchanged, as indicated by the arrows. It seems that the lithium dendrites were etched while plating. A proposed "etching" scheme is schematically illustrated in Figure S9 (Supporting Information).

To further understand the polysulfide "etching" mechanism, we studied the formation energy per lithium atom, ε_f(Li), in lithium polysulfide clusters and in lithium metal using density functional theory (DFT). Note that a structure with a lower ε_f(Li) forms more easily under a certain chemical environment. For lithium polysulfide clusters $S_{n_S}Li_{n_{Li}}$, ε_f(Li) can be defined as

$$\varepsilon_f(\mathrm{Li}) = \frac{1}{n_{\mathrm{Li}}}[E(S_{n_S}Li_{n_{Li}}) - n_S\mu_S - n_{Li}\mu_{Li\ bulk}] \quad (1)$$

where $E(S_{n_S}Li_{n_{Li}})$ is the total energy of the cluster, and n_S and n_{Li} are the numbers of sulfur and lithium atoms in the cluster, respectively. $\mu_{Li\ bulk}$ is the chemical potential of lithium in its bulk. μ_S is the chemical potential of sulfur, which can be considered in balance with the environment/electrolyte. A more negative value of μ_S corresponds to an S-deficient environment/electrolyte which tends to take in more sulfur and hinders the Li atoms to capture these S atoms, yielding a higher formation energy of $S_{n_S}Li_{n_{Li}}$ clusters but easy formation of Li bulk/dendrites.

Figure 4a shows ε_f(Li) as a function of the chemical potential of sulfur, μ_S. It can be seen that the lowest ε_f(Li) configurations change in different environments/electrolytes reflected in the values of μ_S. When μ_S is smaller than –0.60 eV, corresponding to a Li-rich environment, lithium in its bulk form is the most energetically favorable (ε_f(Li) = 1.896 eV), as shown by the horizontal black line in Figure 4a. When μ_S gradually increases which means the gradual accumulation of sulfur atoms in the environment/electrolytes, it can be found that Li_2S_3, Li_2S_4, Li_2S_6, and Li_2S_8 clusters become the most stable

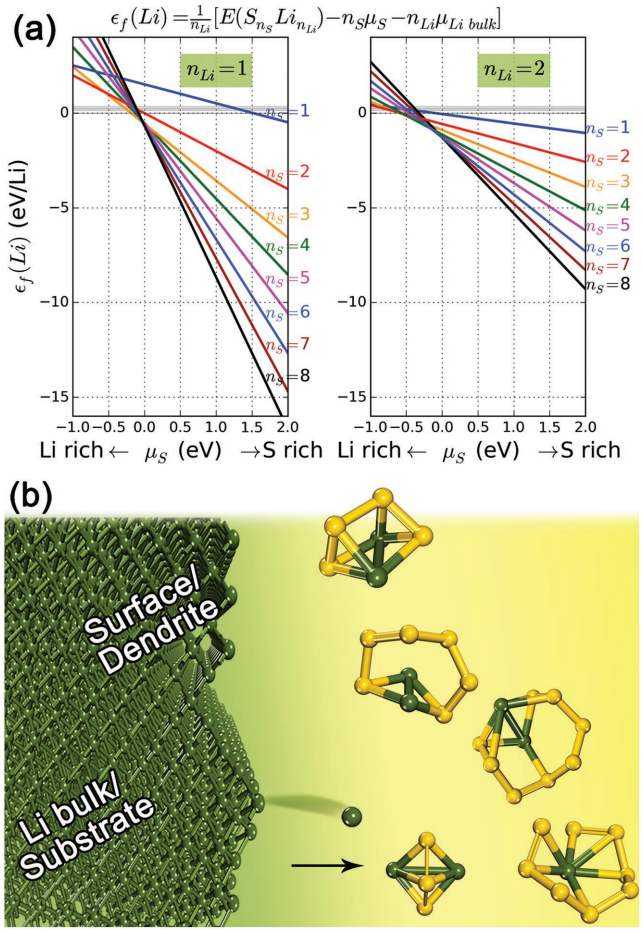

Figure 4. a) The formation energy per Li atom, ε_f(Li), in the cluster $S_{n_S}Li_{n_{Li}}$ ($1 \le n_S \le 8$, $n_{Li} = 1,2$) as functions of the chemical potential of sulfur (μ_S), where that of sulfur in S_8 bulk is set to zero. The horizontal black line is the energies of Li in Li metal. b) A schematic view of changing the chemical environment of the electrolyte that leads to different lowest ε_f(Li) structures, which are Li bulk, Li_2S_3, Li_2S_4, Li_2S_6, Li_2S_8, and LiS_8, from Li-rich (green) to S-rich (yellow), respectively.

structures at $\mu_S = -0.60$, -0.48, -0.16, and 0.00 eV, respectively, as shown in Figure 4b. It is in agreement with previous theoretical[35] and experimental[36] studies on polysulfide clusters that Li_2S_n ($n = 3, 4, 6, 8$) clusters have superior stability. The exact form of polysulfide clusters depends on the electrolyte environment μ_S.

The above results suggest that adding sulfur into the environment/electrolytes can decelerate the deposition rate of Li atoms on electrode. This is important for suppressing lithium dendrite formation, because a sustainable lithium dendrite growth requires the deposition rate of Li atoms be faster than their diffusion rate on the electrode surface. When a certain amount of sulfur is added to the electrolyte, it becomes more energetically favorable for Li atoms to stay in lithium polysulfide clusters than in Li metal/electrode. The difference of ε_f(Li) in metal/electrode surface and in clusters provides a larger chemical driving force to move Li atoms from dendrite/surface to clusters (solid to liquid), than from dendrite/surface to bulk/substrate (solid to solid), as shown in Figure 4b. Therefore, lithium polysulfide clusters could etch lithium dendrites. As the lithium plating process is controlled by both thermodynamic and kinetic conditions, the coexistence of growth and etching of lithium dendrite is observed.

Based on the above understanding, we further investigated the synergistic dendrite suppression effect of Li_2S_8 (0.2 M) and $LiNO_3$ (1 wt%) co-additives in the LiTFSI/DOL/DME electrolyte. As shown in the false-colored EC-SEM image series of the lithium plating process (**Figure 5**, see also the original gray-scale images in Figure S10 (Supporting Information) and the corresponding video in Movie S4 (Supporting Information)), competing dendrite growth and dissolution were observed. During the whole plating process, the lengths of the lithium dendrites were restrained well below 3 µm, which were much shorter than those formed in the electrolyte with only $LiNO_3$ additive (Figure 2c) or with only Li_2S_8 additive (Figure 3d). To verify the dendrite suppression effect we observed in our in situ EC-SEM experiments, we also performed corresponding ex situ experiments using a coin cell made of a lithium metal anode, a sulfur–graphene cathode, and a LiTFSI/DOL/DME electrolyte with both Li_2S_8 and $LiNO_3$ additives. The coin cell was cycled over 50 cycles, and sequentially disassembled for ex situ SEM investigation. We found that the Li surface was smooth and no lithium dendrite was observed (Figure S11, Supporting Information). These results confirm that the lithium dendrites can be effectively suppressed with the addition of both lithium polysulfide and $LiNO_3$ in the LiTFSI/DOL/DME electrolyte.

The EC-SEM liquid cell developed in this work enables the in situ characterization of electrode materials in volatile ether-based electrolyte which is widely used in lithium/sulfur batteries, and thus well mimics the real operating environment of a battery. Despite the low atomic number, lithium could be clearly imaged in SEM as dark contrast on the slightly charged SiN_x membrane background, and thus the growth and dissolution of lithium dendrites could be tracked. This in situ SEM technique offers an intermediate spatial resolution between that of the in situ TEM and the in situ optical microscopy. Compared to an in situ TEM cell, adequate amount of electrode and electrolyte materials can be contained in the EC-SEM liquid cell, allowing a better cycle performance (typically more than 15 cycles in this study, better than that of a TEM liquid cell which is no more than ten cycles in the literature[19]). The resolution of in situ SEM in this work is limited due to the electron beam broadening effect of the SiN_x membrane (see Figure S12, Supporting Information), which is more serious when the electron beam energy is set as low as 10 keV (we used a low electron beam energy in order to protect the SiN_x membrane from fracturing). It is also noteworthy that a relatively lower energy electron beam results in a smaller penetration length in the sample, and thus, only those lithium dendrites lying close to the SiN_x membrane could be imaged. The smaller penetration depth, at least in our case, avoids the complex beam–liquid interaction and provides useful morphology information near the surface.

In this work, caution has been taken to exclude any possible electron beam effect during the in situ SEM experiments. We normally recorded extra images outside the continuously scanned area after the in situ experiments to

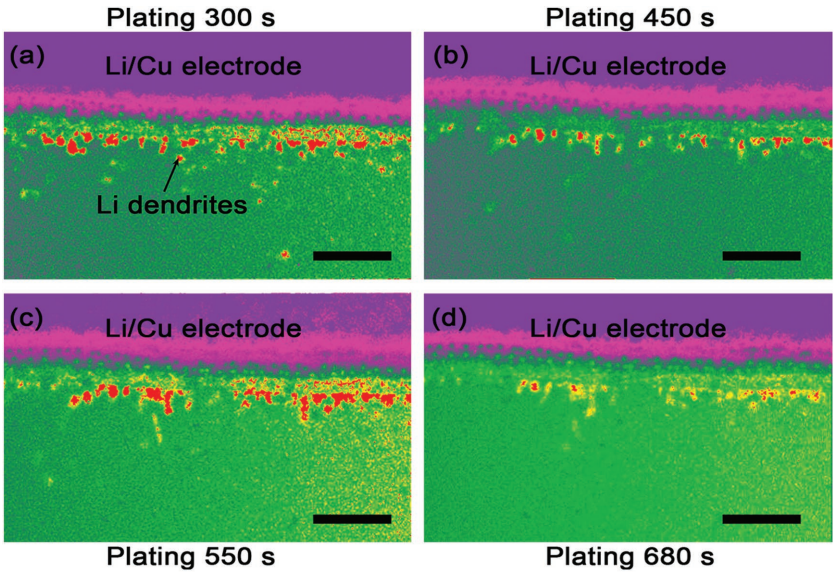

Figure 5. a–d) A time lapse series of SEM images of the lithium plating process under 0.15 mA cm^{-2} on the Li/Cu electrode using the LiTFSI/DOL/DME electrolyte with the addition of both Li_2S_8 (0.2 M) and $LiNO_3$ (1 wt%). The artificial colors of purple-green-yellow-red represent the different contrasts from bright to dark in grayscale. The dark contrasts of lithium dendrites are colored in red and yellow. Scale bar: 10 μm.

confirm the observed sample features are the same in the areas with/without continuous electron beam scanning. In situ optical microscopy experiments were also conducted in parallel using the same liquid EC-SEM cells to exclude the beam effect. For example, the same lithium dendrite suppression effect of the Li_2S_8-$LiNO_3$-LiTFSI/DOL/DME electrolyte was also observed using the in situ optical microscopy (as shown in Movie S5, Supporting Information). Therefore, despite that the charging effect was observed in a few in situ SEM experiments, the beam effect was mostly minimized to a negligible impact on the electrode evolution during the EC-SEM cell's operation.

Despite the earlier reports that polysulfides could play an important role in the formation of a stable SEI film on the Li electrode, thus preventing lithium dendrites growth in Li/S batteries,[14,29,32,37] here, both our in situ experimental result and the theoretical calculation strongly suggest that the lithium polysulfides actually limit the growth of dendrite by an "etching" reaction with them. Our results further demonstrate that the co-addition of both $LiNO_3$ and Li_2S_8 in the electrolyte can effectively suppress the lithium dendrite growth due to the synergetic effect toward the reaction with Li electrode. First, $LiNO_3$ could boost at least a partial formation of a SEI film and slow down the dendrite growth (see Figure S5, Supporting Information); second, those relatively short dendrites can be further chemically etched by lithium polysulfides, leading to a smoother surface of the Li anode.

In summary, a liquid EC-SEM cell is developed for in situ investigation of the lithium plating/stripping processes in ether-based electrolyte. The lithium dendrite growth, dissolution, and the "dead" Li formation processes were clearly observed in real time and the results show that the lithium dendrites can be effectively suppressed by Li_2S_8 and $LiNO_3$ as co-additives in the electrolyte. The in situ liquid phase EC-SEM technique thus provides a powerful tool for the study of fundamental electrochemical processes in lithium batteries. It should also have a great application potential in understanding the mechanisms of many other electrochemical systems.

Supporting Information

Supporting Information is available from the Wiley Online Library or from the author.

Acknowledgements

G.R. and X.Z. contributed equally to this work. This work was supported by the National Natural Science Foundation of China (21433013), the National Key Research and Development Program of China (2016YFB0100100), the CAS-DOE Joint Research Program (121E32KYSB20150004), and Beijing Municipal Science and Technology Commission (D161100002416003).

Received: November 17, 2016
Revised: December 15, 2016
Published online:

[1] M. N. Liu, F. M. Ye, W. F. Li, H. F. Li, Y. G. Zhang, *Nano Res.* **2016**, *9*, 94.
[2] S. P. Wu, R. Xu, M. J. Lu, R. Y. Ge, J. Iocozzia, C. P. Han, B. B. Jiang, Z. Q. Lin, *Adv. Energy Mater.* **2015**, *5*, 1.
[3] M. K. Song, E. J. Cairns, Y. G. Zhang, *Nanoscale* **2013**, *5*, 2186.
[4] P. G. Bruce, S. A. Freunberger, L. J. Hardwick, J. M. Tarascon, *Nat. Mater.* **2012**, *11*, 19.
[5] J. Hassoun, K. S. Lee, Y. K. Sun, B. Scrosati, *J. Am. Chem. Soc.* **2011**, *133*, 3139.
[6] B. Kumar, J. Kumar, R. Leese, J. P. Fellner, S. J. Rodrigues, K. M. Abraham, *J. Electrochem. Soc.* **2010**, *157*, A50.
[7] A. Zhamu, G. R. Chen, C. G. Liu, D. Neff, Q. Fang, Z. N. Yu, W. Xiong, Y. B. Wang, X. Q. Wang, B. Z. Jang, *Energy Environ. Sci.* **2012**, *5*, 5701.
[8] H. Kim, G. Jeong, Y. U. Kim, J. H. Kim, C. M. Park, H. J. Sohn, *Chem. Soc. Rev.* **2013**, *42*, 9011.
[9] W. Xu, J. L. Wang, F. Ding, X. L. Chen, E. Nasybutin, Y. H. Zhang, J. G. Zhang, *Energy Environ. Sci.* **2014**, *7*, 513.
[10] D. Aurbach, *J. Power Sources* **2000**, *89*, 206.
[11] Z. Zeng, X. Zhang, K. Bustillo, K. Niu, C. Gammer, J. Xu, H. Zheng, *Nano Lett.* **2015**, *15*, 5214.
[12] F. Wu, N. Yao, *Nano Energy* **2015**, *11*, 196.
[13] Y. C. Qiu, G. L. Rong, J. Yang, G. Z. Li, S. Ma, X. L. Wang, Z. H. Pan, Y. Hou, M. N. Liu, F. M. Ye, W. F. Li, Z. W. Seh, X. Y. Tao, H. B. Yao, N. Liu, R. F. Zhang, G. M. Zhou, J. P. Wang, S. S. Fan, Y. Cui, Y. G. Zhang, *Adv. Energy Mater.* **2015**, *5*, 1.
[14] W. Li, H. Yao, K. Yan, G. Zheng, Z. Liang, Y. M. Chiang, Y. Cui, *Nat. Commun.* **2015**, *6*, 7436.
[15] H. Ghassemi, M. Au, N. Chen, P. A. Heiden, R. S. Yassar, *Appl. Phys. Lett.* **2011**, *99*, 123113.

[16] X. H. Liu, L. Zhong, L. Q. Zhang, A. Kushima, S. X. Mao, J. Li, Z. Z. Ye, J. P. Sullivan, J. Yu, *Appl. Phys. Lett.* **2011**, *98*, 183107.
[17] Z. Zeng, W. I. Liang, H. G. Liao, H. L. Xin, Y. H. Chu, H. Zheng, *Nano Lett.* **2014**, *14*, 1745.
[18] A. J. Leenheer, K. L. Jungjohann, K. R. Zavadil, J. P. Sullivan, C. T. Harris, *ACS Nano* **2015**, *9*, 4379.
[19] C. M. Wang, *J. Mater. Res.* **2014**, *30*, 326.
[20] X. B. Cheng, H. J. Peng, J. Q. Huang, R. Zhang, C. Z. Zhao, Q. Zhang, *ACS Nano* **2015**, *9*, 6373.
[21] T. Osaka, T. Homma, T. Momma, H. Yarimizu, *J. Electroanal. Chem.* **1997**, *421*, 153.
[22] P. C. Howlett, D. R. MacFarlane, A. F. Hollenkamp, *J. Power Sources* **2003**, *114*, 277.
[23] K. Nishikawa, T. Mori, T. Nishida, Y. Fukunaka, M. Rosso, T. Homma, *J. Electrochem. Soc.* **2010**, *157*, A1212.
[24] K. Nishikawa, H. Naito, M. Kawase, T. Nishida, *J. Electrochem. Soc.* **2012**, *41*, 3.
[25] J. Steiger, D. Kramer, R. Moenig, *Electrochim. Acta* **2014**, *136*, 529.
[26] Z. Liang, G. Zheng, C. Liu, N. Liu, W. Li, K. Yan, H. Yao, P. C. Hsu, S. Chu, Y. Cui, *Nano Lett.* **2015**, *15*, 2910.
[27] G. Zheng, S. W. Lee, Z. Liang, H. W. Lee, K. Yan, H. Yao, H. Wang, W. Li, S. Chu, Y. Cui, *Nat. Nanotechnol.* **2014**, *9*, 618.
[28] F. Wu, J. Qian, R. Chen, J. Lu, L. Li, H. Wu, J. Chen, T. Zhao, Y. Ye, K. Amine, *ACS Appl. Mater. Interfaces* **2014**, *6*, 15542.
[29] S. Xiong, K. Xie, Y. Diao, X. Hong, *J. Power Sources* **2013**, *236*, 181.
[30] L. Suo, Y. S. Hu, H. Li, M. Armand, L. Chen, *Nat. Commun.* **2013**, *4*, 1.
[31] F. Ding, W. Xu, G. L. Graff, J. Zhang, M. L. Sushko, X. L. Chen, Y. Y. Shao, M. H. Engelhard, Z. Nie, J. Xiao, X. J. Liu, P. V. Sushko, J. Liu, J. G. Zhang, *J. Am. Chem. Soc.* **2013**, *135*, 4450.
[32] D. Aurbach, E. Pollak, R. Elazari, G. Salitra, C. S. Kelley, J. Affinito, *J. Electrochem. Soc.* **2009**, *156*, A694.
[33] Y. Zhang, A. Chang, J. Cao, Q. Wang, W. Kim, Y. Li, N. Morris, E. Yenilmez, J. Kong, H. Dai, *Appl. Phys. Lett.* **2001**, *79*, 3155.
[34] C. Barchasz, J. C. Lepretre, F. Alloin, S. Patoux, *J. Power Sources* **2012**, *199*, 322.
[35] W. Zhao, P. Chen, P. Tang, Y. Li, J. Wu, W. Duan, *Appl. Phys. Lett.* **2014**, *104*, 043901.
[36] M. Vijayakumar, N. Govind, E. Walter, S. D. Burton, A. Shukla, A. Devaraj, J. Xiao, J. Liu, C. Wang, A. Karim, S. Thevuthasan, *Phys. Chem. Chem. Phys.* **2014**, *16*, 10923.
[37] S. Xiong, K. Xie, Y. Diao, X. Hong, *J. Power Sources* **2014**, *246*, 840.